Supplemental Material to:

The 1:2 complex between RavZ and LC3 reveals a mechanism for deconjugation of LC3 on the phagophore membrane

Do Hoon Kwon[a,1], Sulhee Kim[b,1], Yang Ouk Jung[a], Kyung-Hye Roh[a], Leehyun Kim[a], Byeong-Won Kim[a], Seung Beom Hong[a], In Young Lee[a], Ju Han Song[a], Woo Cheol Lee[b], Eui-Ju Choi[a], Kwang Yeon Hwang[b,*] & Hyun Kyu Song[a,*]

[a]Department of Life Sciences and [b]Division of Biotechnology, Korea University, 145 Anam-ro, Seongbuk-gu, Seoul 02841, Korea

[1]These authors contributed equally to this work.

*Correspondence should be addressed to Hyun Kyu Song (hksong@korea.ac.kr) or Kwang Yeon Hwang (chahong@korea.ac.kr)

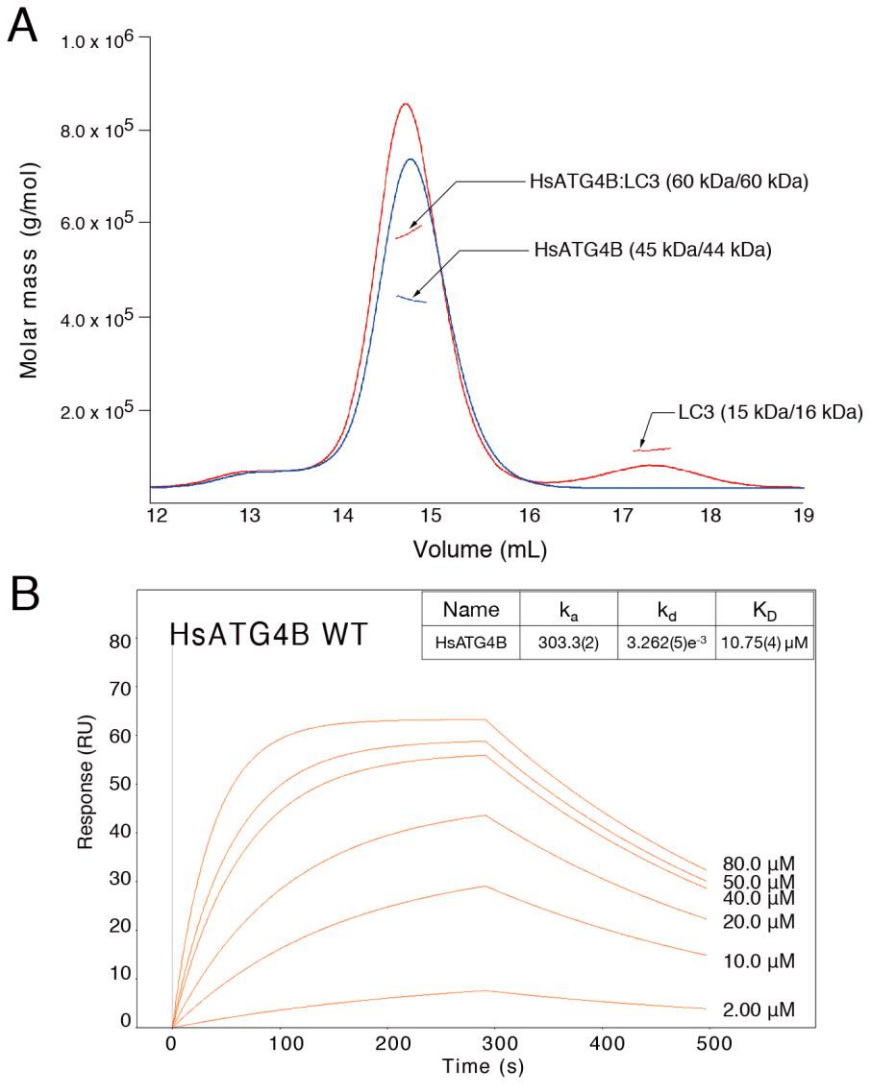

Figure S1. Interaction between ATG4B and LC3. (**A**) The ATG4B-LC3 complex (red line) and ATG4B alone (blue line) analyzed by SEC-MALS. The horizontal line represents the measured MM. Each species is indicated by an arrow with experimental (MALS) and theoretically calculated (Calc) molar mass values shown in parentheses (MALS/Calc). The data show the 1:1 binding stoichiometry between ATG4B and LC3. (**B**) SPR sensorgram for the binding of ATG4B to immobilized LC3 on the PEG chip. The equilibrium dissociation constant (K_D) value between ATG4B and LC3 is 10.75 µM.

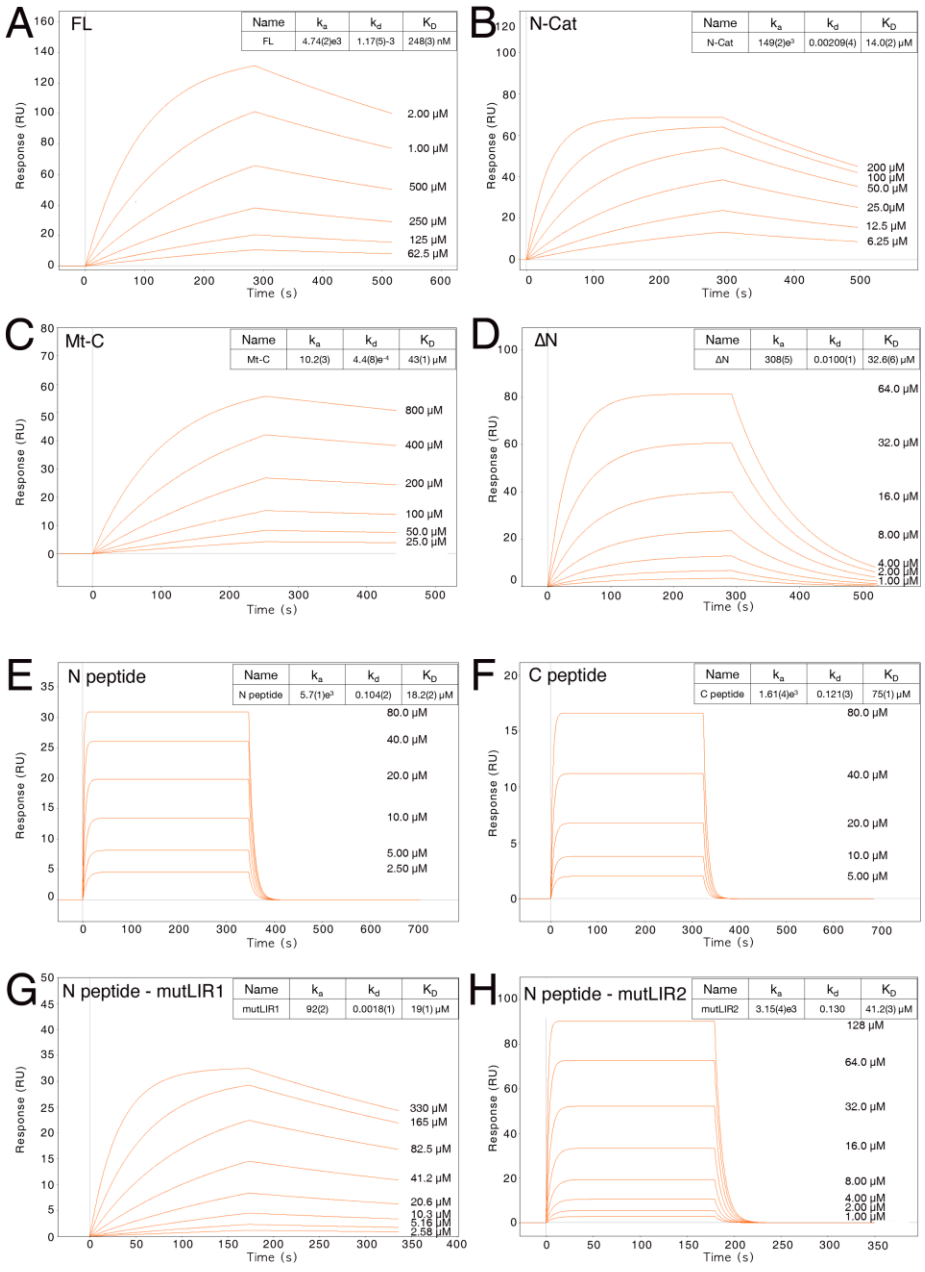

Figure S2. Binding constant measurements by surface plasmon resonance (SPR). SPR sensorgram for the binding of RavZ WT (FL) (**A**), N-Cat (**B**), MT-C (**C**), ΔN (**D**), N-term peptide containing LIR1 and LIR2 (**E**), C-term peptide containing LIR3 (**F**), N-term peptide containing only functional LIR2, mutLIR1 (**G**), and N-term peptide containing only functional LIR1, mutLIR2 (**H**) to immobilized LC3 on the PEG chip. Response (RU, resonance units) is plotted against time. The K_D (dissociation constant) was derived from at least 5 different concentrations of ligand. The results are summarized in **Fig. 1D**.

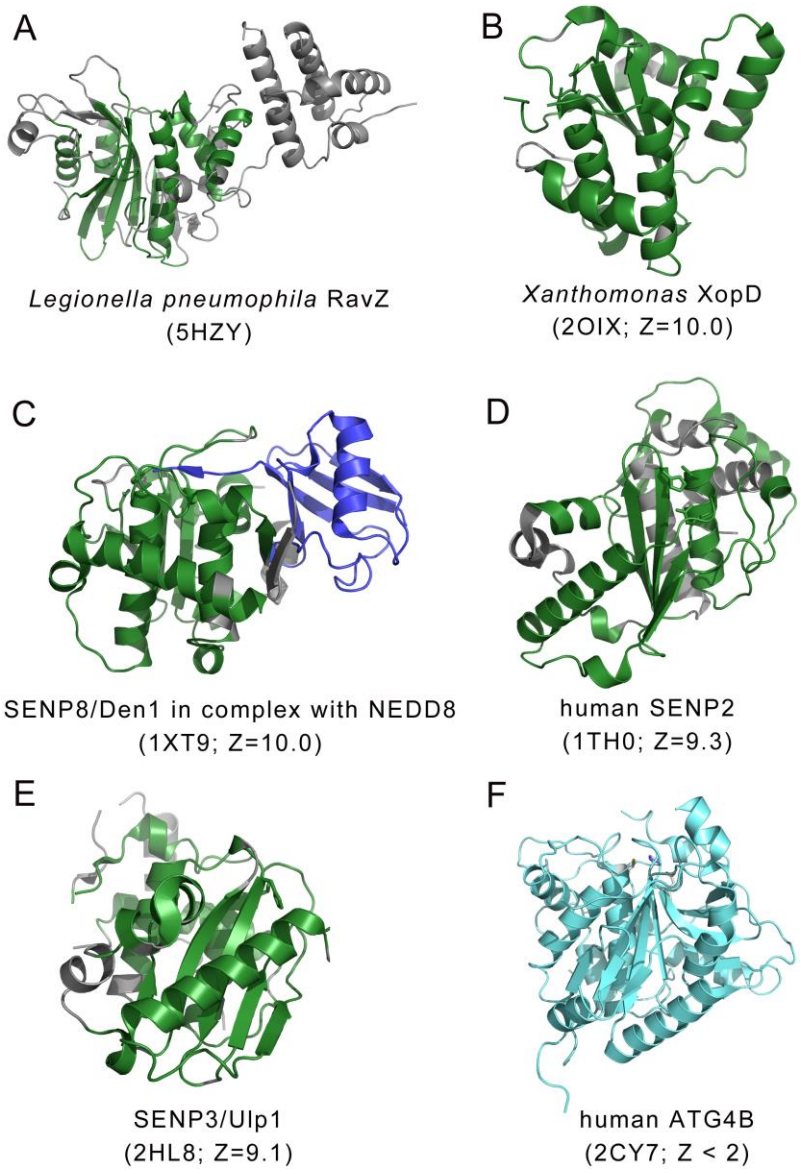

Figure S3. Comparison of the overall structure of RavZ with that of other Ubl proteases. Ribbon diagrams comparing the overall structures of RavZ (**A**), XopD from *Xanthomonas* (**B**), SENP8/Den1 in complex with NEDD8 (**C**), human SENP2 (**D**), SENP3/Ulp1 (**E**), and human ATG4B (**F**). The view represents an approximate 90° rotation of **Fig. 2A** along the horizontal axis to clarify the region. Structural regions that match the corresponding region of RavZ are colored green in each structure. A bound NEDD8 molecule in panel (**C**) is colored blue and structurally dissimilar (Z-score below 2) human ATG4B in panel (**F**) is colored cyan. PDB ID codes and Z-scores from the DALI server for each structure are shown below each structure.

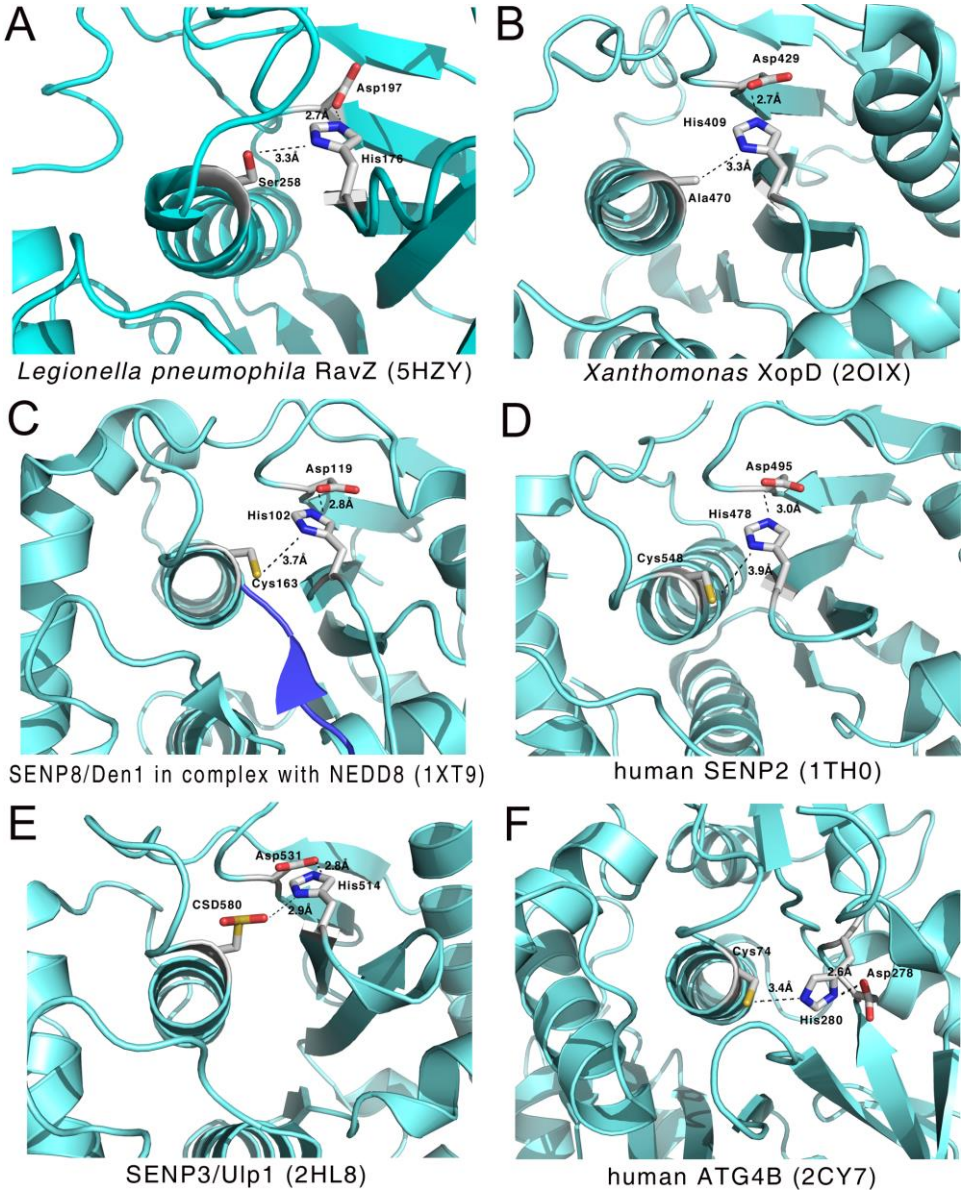

Figure S4. Comparison of the active site of RavZ with that of other Ubl proteases. The models compared are the same as in **Fig. S3**. Side-chains of the catalytic triad are shown as stick models. Carbon, nitrogen, oxygen and sulfur atoms are colored gray, blue, red and yellow, respectively. The catalytic cysteine residue is mutated to serine or alanine in some of the structures.

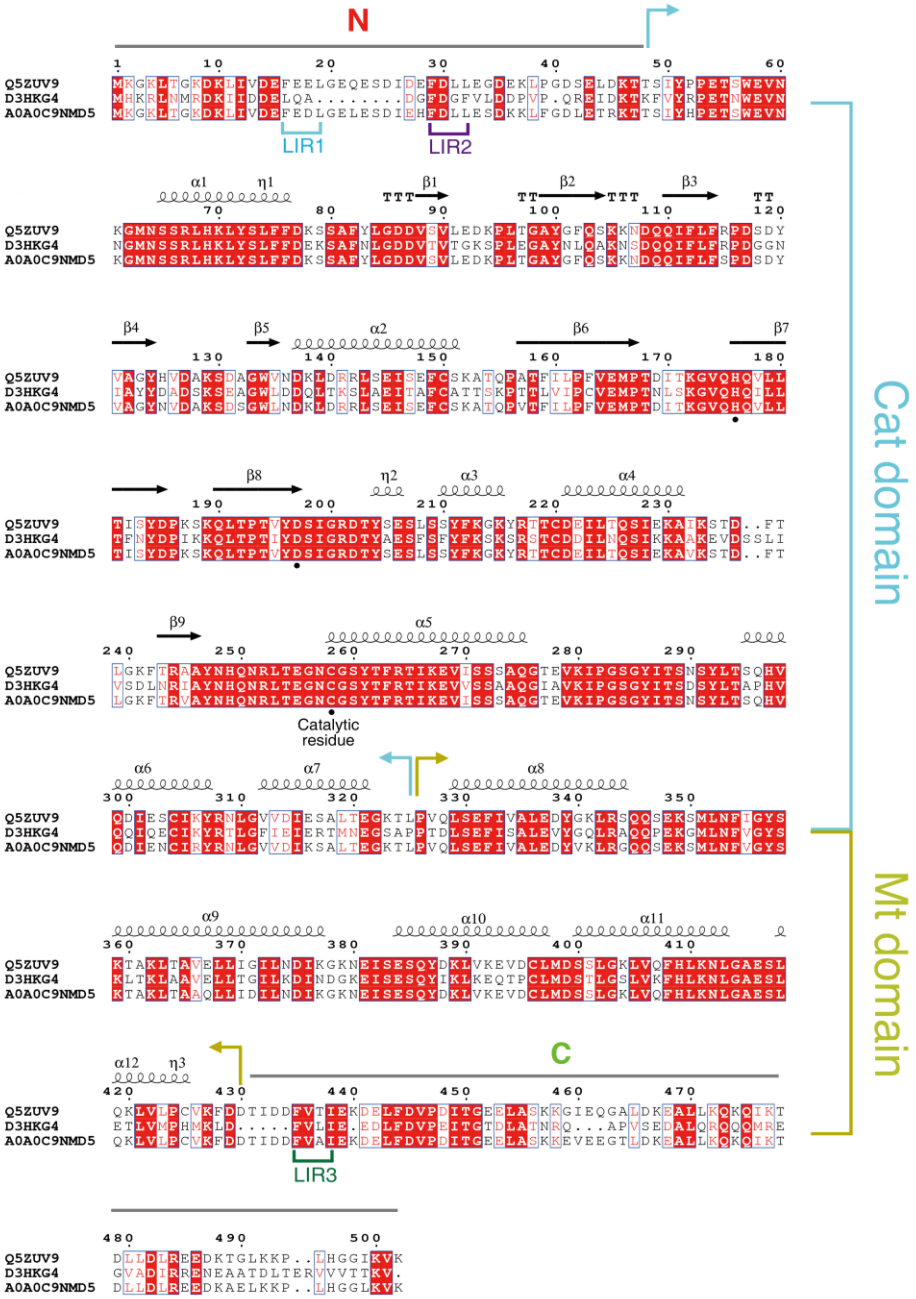

Figure S5. Sequence alignment of RavZ homologs. Q5ZUV9, D3HKG4 and A0A0C9NMD5 are RavZ homologs from *Legionella* species deposited in the UniProt DB. The RavZ domains are indicated. Boxes indicate residues that are identical (red shading) or highly conserved (red font) in all sequences. Secondary structural elements are shown above the sequence alignment and every 10th residue of RavZ from *L. pneumophila* (the 1st row) is marked with a dot and labeled. Residues responsible for the enzyme catalytic activity are marked with black circles. Potential LIR motifs are also indicated.

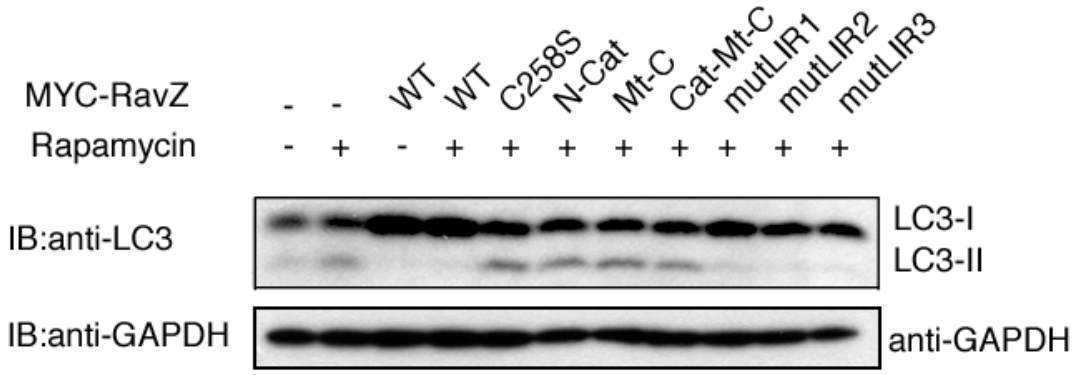

Figure S6. Western blot analyses detecting LC3 turnover. HEK293 cells were transfected with expression vectors comprising the indicated MYC-tagged RavZ variants (wild-type, C258S, N-Cat, Mt-C, Cat-Mt-C, mutLIR1, mutLIR2 and mutLIR3). After 24 h of transfection, cells were left untreated or treated with 1 μM rapamycin for 4 h and then lysed. The lysates were subjected to immunoblot analysis using antibodies to LC3B. GAPDH is used as a loading control.

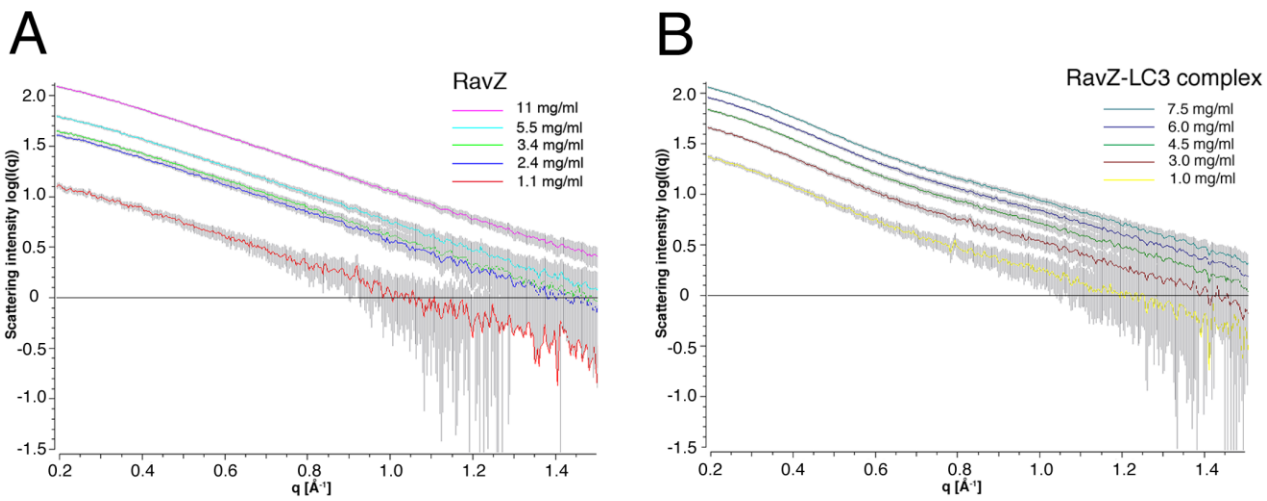

Figure S7. Experimental solution scattering data. Guinier plot of the scattering intensity from SAXS data collected at different concentrations of free RavZ and the RavZ-LC3 complex. (**A**) Plots of the scattering intensity from SAXS data collected at different concentrations of RavZ protein: 11.0 (magenta), 5.5 (cyan), 3.4 (green), 2.4 (blue), and 1.1 mg/ml (red). (**B**) Plots of the scattering intensity from SAXS data collected at different concentrations of the RavZ-LC3 complex: 7.5 (turquoise), 6.0 (blue), 4.5 (green), 3.0 (magenta), and 1.0 mg/ml (yellow).

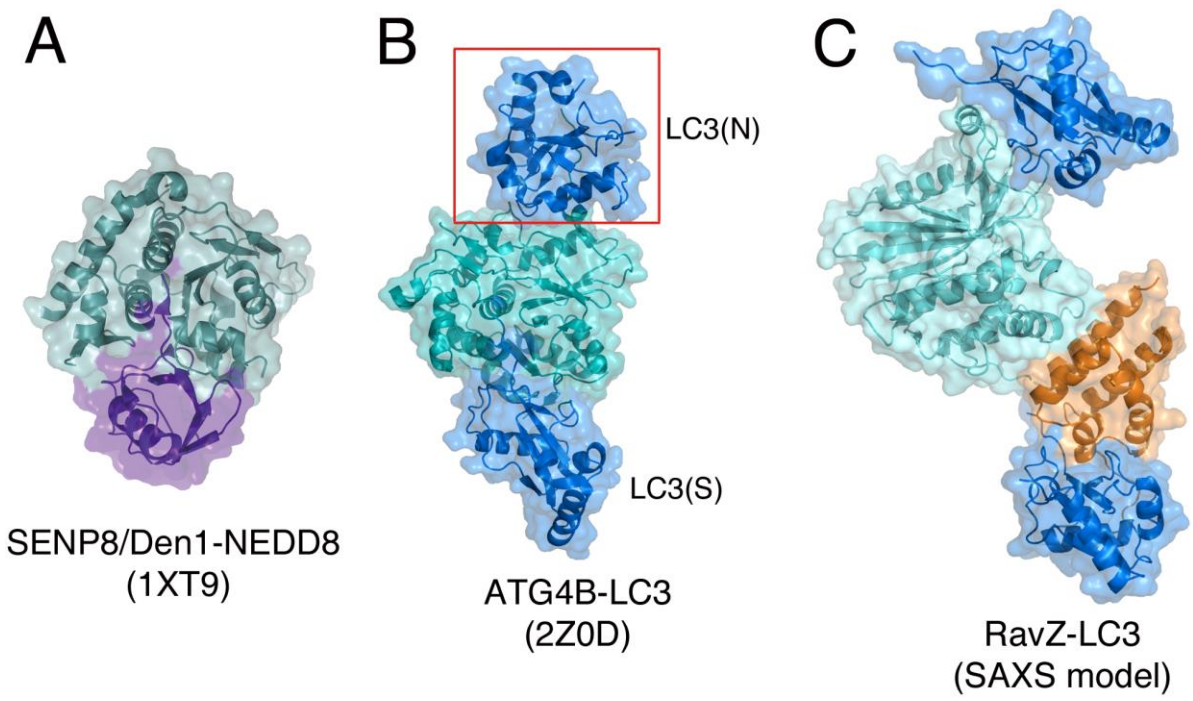

Figure S8. Comparison of the RavZ-LC3 complex model with Ubl protease-substrate and the ATG4B-LC3 complex. (**A**) Structure of the complex between SENP8/Den1 protease and NEDD8 (purple). The C-terminal tail of substrate NEDD8 extends into the active site of the SENP8 protease. (**B**) Structure of the complex between ATG4B and LC3. LC3(S) indicates a substrate LC3, while LC3(N) indicates a nonsubstrate LC3 (red box). Since LC3(S) and LC3(N) are symmetry equivalent molecules in the ATG4B-LC3 complex crystal,[1] the actual complex is 1:1, as also observed in solution (**Fig. S1A**). The C-terminal tail of LC3(S) extends into the active site of ATG4B, whereas LC3(N) binds to the LIR motif of ATG4B. The PDB ID codes are shown in parentheses (**A, B**). (**C**) SAXS-based 1:2 complex model of RavZ-$(LC3)_2$. LC3 molecules are located at the N- and C-terminal regions of RavZ. Both LC3 molecules bind to the LIR motifs of RavZ.

Table S1. SAXS data collection and analysis.

Data collection parameters	RavZ	RavZ-LC3
Beamline	PAL 4C	PF BL10C
Beam geometry	20 mm slit	1.6 mm x 8 mm
Wavelength (Å)	1.240	1.488
q range ($Å^{-1}$)	0.001 – 0.3	0.001 – 0.27
Exposure time (s)	60	5
Concentration range (mg ml^{-1})	0.5 – 20	1 – 20
Temperature (K)	289	289
Structural parameters		
I(0) (cm^{-1}) [From P(r)]	0.210	0.207
R_g (Å) [From P(r)]	36.20 ± 0.36	43.47 ± 0.38
I(0) (cm^{-1}) [From Guinier]	0.220 ± 0.012	0.199 ± 0.003
R_g (Å) [From Guinier]	36.2 ± 2.4	43.5 ± 2.6
D_{max} (Å)	121.9	145.9
Porod volume estimate, Vp ($Å^3$)	70472.2	121248.0
Dry volume calculated from sequence ($10^3 Å^3$)	68.0	84.6
Molecular mass determination		
Molecular mass M_r [From Porod volume (Vp*0.66)]	46981.5	80832.0
Calculated monomeric Mr from sequence	56241.5	84464.0
Software employed		
Primary data reduction	In-house program	FIT2D
Data processing	PRIMUS	
Ab initio analysis	DAMMIN	
Validation and averaging	DAMAVER	
Rigid-body modeling	Situs program suite	
Computation of model intensities	PyMOL/Chimera	

Supplementary Reference

[1] Satoo K, Noda NN, Kumeta H, Fujioka Y, Mizushima N, Ohsumi Y, Inagaki F. The structure of Atg4B-LC3 complex reveals the mechanism of LC3 processing and delipidation during autophagy. EMBO J 2009; 28:1341-50.